METABOLISM AND BIOENERGETICS:

Mutations in Both Sides of the Photosystem I Reaction Center Identify the Phylloquinone Observed by Electron Paramagnetic Resonance Spectroscopy

Brent Boudreaux, Fraser MacMillan, Christian Teutloff, Rufat Agalarov, Feifei Gu, Stéphane Grimaldi, Robert Bittl, Klaus Brettel and Kevin Redding

J. Biol. Chem. 2001, 276:37299-37306.
doi: 10.1074/jbc.M102327200 originally published online August 6, 2001

THE JOURNAL OF BIOLOGICAL CHEMISTRY
Vol. 276, No. 40, Issue of October 5, pp. 37299–37306, 2001

Printed in U.S.A.

Mutations in Both Sides of the Photosystem I Reaction Center Identify the Phylloquinone Observed by Electron Paramagnetic Resonance Spectroscopy*

Received for publication, March 15, 2001, and in revised form, July 24, 2001
Published, JBC Papers in Press, August 6, 2001, DOI 10.1074/jbc.M102327200

Brent Boudreaux‡, Fraser MacMillan§, Christian Teutloff¶, Rufat Agalarov‖, Feifei Gu‡, Stéphane Grimaldi§, Robert Bittl¶, Klaus Brettel‖, and Kevin Redding‡**

From the ‡Departments of Chemistry and Biological Sciences, University of Alabama, Tuscaloosa, Alabama 35487, §Institut für physikalische und theoretische Chemie, Marie Curie Strasse 11, J. W. Goethe Universität, D-60439 Frankfurt am Main, Germany, ¶Max-Volmer-Institut, Technische Universität Berlin, Strasse des 17. Juni 135, D-10623 Berlin, Germany, and ‖Section de Bioénergétique and CNRS URA 2096, Département de Biologie Cellulaire et Moléculaire, Commissariat à l'Energie Atomique, Saclay, Bâtiment 532, 91191 Gif-sur-Yvette, France

The core of photosystem I (PS1) is composed of the two related integral membrane polypeptides, PsaA and PsaB, which bind two symmetrical branches of cofactors, each consisting of two chlorophylls and a phylloquinone, that potentially link the primary electron donor and the tertiary acceptor. In an effort to identify amino acid residues near the phylloquinone binding sites, all tryptophans and histidines that are conserved between PsaA and PsaB in the region of the 10th and 11th transmembrane α-helices were mutated in *Chlamydomonas reinhardtii*. The mutant PS1 reaction centers appear to assemble normally and possess photochemical activity. An electron paramagnetic resonance (EPR) signal attributed to the phylloquinone anion radical (A_1^-) can be observed either transiently or after illumination of reaction centers with pre-reduced iron-sulfur clusters. Mutation of PsaA-Trp^{693} to Phe resulted in an inability to photo-accumulate A_1^-, whereas mutation of the analogous tryptophan in PsaB (PsaB-Trp^{673}) did not produce this effect. The PsaA-W693F mutation also produced spectral changes in the time-resolved EPR spectrum of the P_{700}^+ A_1^- radical pair, whereas the analogous mutation in PsaB had no observable effect. These observations indicate that the A_1^- phylloquinone radical observed by EPR occupies the phylloquinone-binding site containing PsaA-Trp^{693}. However, mutation of either tryptophan accelerated charge recombination from the terminal Fe-S clusters.

Photosystem I (PS1)[1] is a multisubunit membrane protein in the thylakoid membrane of green plants and cyanobacteria. It converts electromagnetic energy into chemical energy by using photons to drive electron transfer between electron carriers on opposite sides of the membrane. The core of PS1 is a heterodimer of two subunits, PsaA and PsaB. These polypeptides are related to each other, sharing 45–50% identical residues, and each contains 11 transmembrane α-helices (1, 2). The first six transmembrane helices bind chlorophyll (Chl) molecules of the core antenna, and the last five helices form a framework holding the cofactors involved in transmembrane electron transfer (Refs. 3 and 4; see Fig. 1). In order, the cofactors are: P_{700} (pair of Chl *a* molecules), A_0 (Chl *a*), A_1 (phylloquinone), and F_X (Fe_4S_4 cluster). The terminal electron acceptors, F_A and F_B (Fe_4S_4 clusters), are bound by the PsaC subunit. Upon excitation of P_{700}, an electron is transferred to A_0, subsequently to A_1, through the iron-sulfur clusters, and ultimately to ferredoxin.

The function of phylloquinone in electron transfer in PS1 is based, among others, on the observation of a transient optical difference spectrum with features similar to that of the phyllosemiquinone-phylloquinone difference spectrum. This optical feature decays with a half-time of 200 ns (3), which is in line with measurements of A_1^- reoxidation by time-resolved EPR (4–6) and photovoltage analysis (7). A faster phase of A_1^- reoxidation has also been observed in PS1 from spinach ($t_{1/2}$ = 15–25 ns; Refs. 8 and 9) and cyanobacteria ($t_{1/2}$ = 7 ns; Ref. 10). Recent *in vivo* optical studies in green algae led to the suggestion that the two phases of A_1^- reoxidation reflect the existence of two parallel, but kinetically distinct, electron transfer pathways from P_{700} to F_X (11), in line with the presence of two phylloquinone molecules in PS1 (12).

The singly reduced phyllosemiquinone is a radical and thus accessible to EPR spectroscopy. Two methods have been used to observe the normally transient A_1^- radical: time-resolved spectroscopy and photo-accumulation. Charge separation produces a spin-polarized EPR signal that decays in the nanosecond to microsecond time scales, depending upon the temperature (4, 13). An EPR signal can also be accumulated by illumination at low temperature after reduction of the Fe-S clusters. Its mean *g*-value (2.0045) and ~10-G width were similar to that of semiquinones, and it was assigned to A_1^- (see Ref. 14 and references therein). Spin quantification in cyanobacterial PS1 after photo-accumulation produced a maximum of 1 A_0^- and 1 A_1^- per P_{700} (15, 16), although earlier work with spinach PS1 seemed to be consistent with a maximum of 4 spins per P_{700} (14). Furthermore, the high field EPR spectrum (15) and electron nuclear double resonance (ENDOR) spectra of photo-accumulated A_1^- (17, 18) are most consistent with a unique qui-

* The costs of publication of this article were defrayed in part by the payment of page charges. This article must therefore be hereby marked "*advertisement*" in accordance with 18 U.S.C. Section 1734 solely to indicate this fact.

** Supported by Energy Biosciences Grant DE-FG02-00ER15097 from the Department of Energy. To whom correspondence should be addressed: Depts. of Chemistry and Biological Sciences, University of Alabama, 120 Lloyd Hall, 6th Ave., Tuscaloosa, AL 35487. Tel.: 205-348-8430; Fax: 205-348-9104; E-mail: kevin.redding@mail.ua.edu.

[1] The abbreviations used are: PS1, photosystem I; Chl, chlorophyll; ENDOR, electron-nuclear double resonance; EPR, electron paramagnetic resonance; F_A, iron-sulfur center B; F_B, iron-sulfur center B; F_X, iron-sulfur center X; MS, mass spectrometry; P_{700}, primary donor of photosystem I; PMS, phenazine methosulfate; PS2, photosystem II; WT, wild type; E, einstein(s); ESEEM, electron spin echo envelope modulation; Tricine, *N*-[2-hydroxy-1,1-bis(hydroxymethyl)ethyl] glycine.

none. Moreover, the conformity of the hyperfine couplings measured in both the photo-accumulated and transient A_1^- radicals has allowed the conclusion that they arise from the same molecule on the same side of PS1 (19).

Advanced EPR spectroscopic techniques and x-ray crystallography have provided information on the environment of the quinones. A combination of ^{15}N labeling and electron spin echo envelope modulation (ESEEM) spectroscopy of photo-accumulated A_1^- indicated that a tryptophan (Trp) and perhaps one other nitrogen-containing aromatic side chain were nearby (20). ENDOR spectroscopy of the photo-accumulated A_1^- radical detected an altered electron spin density distribution compared with phyllosemiquinone *in vitro* (17, 18), and it has been suggested that the quinone oxygen(s) are hydrogen-bonded (17), although strong H-bonding would be difficult to reconcile with A_1's low redox potential and the ability of different quinone compounds to insert into the A_1 site in alternate orientations (21). EPR analysis of photo-accumulated A_1^- in oriented PS1 (15) and of the P_{700}^+ A_1^- radical pair in PS1 crystals allowed prediction of the phylloquinone site in the three-dimensional structure (22), and electron densities in this region and the symmetry-related region have been assigned to the two phylloquinones (23). These sites are in an area where the 10th transmembrane α-helices of PsaA and PsaB are linked to an α-helix parallel to the membrane plane (Fig. 1).

Here we describe the analysis of a series of mutations guided by this information. Conserved histidines and tryptophans were targeted in a region most likely to be close to the phylloquinones. A tryptophan in PsaA has been identified that appears to be near A_1, because of the effect of its mutation upon the A_1^- EPR signal. After submission of this paper, the three-dimensional structure of cyanobacterial PS1 at 2.5-Å resolution was published (12). The tryptophan shown here to affect the A_1^- EPR signal turned out to be π-stacked with the phylloquinone bound to PsaA. The phylloquinone bound to PsaB is similarly stacked with the analogous tryptophan (12), but we observed no modification of the A_1^- EPR signal upon mutation of this residue. These results speak to the inherent asymmetry of PS1.

EXPERIMENTAL PROCEDURES

Genetic Techniques—Site-directed mutations were introduced by the three-stage polymerase chain reaction method (24), utilizing a system designed for site-directed mutagenesis of *Chlamydomonas* PsaA and PsaB (25). Mutations in the *psaA* third exon were constructed in pKR154, and mutations in *psaB* were constructed in pKR164. All mutations were confirmed by sequencing. At least two independent subclones of each plasmid were introduced into the appropriate null mutant strains by particle bombardment and selection on spectinomycin-containing medium. Double mutants were created by simultaneously bombarding a strain lacking *psaA-3* and *psaB* with a mixture of two plasmids containing mutations in the same site of *psaA-3* and *psaB*; spectinomycin-resistant transformants were subjected to light (20–50 microeinsteins (μE)/m^2/s) to select for double transformants, as single transformants would lack PS1 and be light-sensitive. Two different genetic backgrounds were used in the creation of mutant strains. A wild-type (WT) background was used for *in vivo* characterization, whereas a background lacking Chl *b* and photosystem II (PS2) was used to simplify PS1 purification for biophysical analyses. Homoplasmicity was assessed by polymerase chain reaction amplification of the affected locus using isolated DNA as template. At least two independent transformants of each plasmid subclone were characterized to ensure that the observed phenotypes were due to the point mutation and not to any secondary mutations.

Growth Conditions and in Vivo Tests—Tris acetate-phosphate and high salt minimal media were prepared according to Harris (26). Algae were grown heterotrophically at 25 °C in liquid Tris acetate-phosphate medium under low illumination. Growth tests were initiated by spotting 10 μl of log phase cultures onto agar plates. These plates were incubated at 25 °C under low (<1 μE/m^2/s), medium (40 μE/m^2/s), or high (200 μE/m^2/s) light fluxes. Anaerobiosis was imposed using the BBL GasPak pouch system (Becton Dickinson Microbiology Systems). Fluorescence induction kinetics were captured with a Plant Efficiency Analyzer (Hansatech Instruments Ltd., Norfolk, United Kingdom). Oxygen evolution was measured with a Hansatech Oxygraph system using a black acetal water-jacketed chamber (maintained at 25 °C) and illuminated by two red LED arrays (650 ± 50 nm; 2700 μE/m^2/s maximum total intensity) at opposite ends of the chamber. Cells were resuspended at 30 μg of Chl/ml in 12.5 mM $NaHCO_3$ (pH 7.5) and introduced into the chamber. Dark O_2 uptake and light-saturated O_2 evolution rates were measured before and after addition of 250 μM *p*-benzoquinone to remove limitations of electron transport beyond PS2.

Preparation and Biochemical Characterization of Membranes, Thylakoids, and PS1 Particles—Crude membrane fractions were prepared as described (27). Thylakoids and PS1 particles were prepared as described (28). Chl concentration was calculated as described (29). PS1 activity in crude membranes was measured using ascorbate and 2,6-dichlorophenol indophenol as donors and methyl viologen as a mediator to oxygen (30). The rate of oxygen reduction was monitored at various light intensities. The PS1-dependent rates of oxygen uptake were determined by subtracting the oxygen uptake level of a sample lacking PS1, and the maximum rates of oxygen uptake were determined by a double-reciprocal plot. Immunoblotting was performed according to a standard protocol using rabbit antisera against PsaA, PsaC, PsaD, PsaE, and PsaF (31).

Liquid Chromatography-Mass Spectrometry (MS) Detection of Phylloquinone—Extracts of pigments from purified PS1 samples were prepared as described (32), except that PS1 particles were used instead of PS2. Separation of phylloquinone was achieved with a Hewlett-Packard series 1050 liquid chromatograph and detected by a PE-Sciex API 3 triple quadrupole mass spectrometer equipped with an atmospheric pressure electrospray source. A full scan mass spectrum of a phylloquinone standard (Sigma) was obtained in the positive ion mode by injection into a 25 μl/min flow of 10 mM ammonium acetate in methanol. MS/MS data of phylloquinone were then obtained by selecting the parent ion peak with the first quadrupole for entry into the second quadrupole. Upon impact with argon there, the parent ions gave rise to fragments that were scanned by the third quadrupole to give the MS/MS spectrum, which formed the basis for the multiple reaction monitoring protocol. Three parent-daughter ion combinations were chosen to detect phylloquinone. Samples were injected onto a 2.1 × 100-mm Aquapore RP-300 reversed phase column (Applied Biosystems) using a flow rate of 0.2 ml/min. The gradient was 30–80% 10 mM ammonium acetate/methanol in 5 min, and then 80% methanol for 10 min, giving a retention time of 12.8 min for the phylloquinone standard.

EPR Spectroscopy of Photo-accumulated A_1^-—Samples were prepared for photo-accumulation of A_1^- as described previously (15). X-band (9.44 GHz) cw-EPR spectra were recorded on a Bruker ESP300 spectrometer using a standard rectangular Bruker EPR cavity (ER4102T). Q-band (34.0 GHz) cw-EPR spectra were measured on a Bruker E-500 spectrometer using a standard Bruker resonator (ER 5106QT-W1). Both instruments were equipped with an Oxford helium cryostat (ESR900 and CF935 respectively). The microwave frequency was measured using a Systron Donner 6054D (X-band) or a Hewlett Packard HP5352b (Q-band) frequency counter. The magnetic field was measured using a Bruker gaussmeter (ER035M). The measured *g*-values were corrected for an offset against a known *g* standard ((2,2′)diphenyl-β-picryl hydroxyl using $g = 2.00351$). The simulated spectrum of A_1^- was generated with Bruker SimFonia (version 1.25) using the *g*-tensor components from the high field EPR spectrum (15), methyl hyperfine coupling taken from the ENDOR spectrum (18), and linewidths of 4 G. The simulated spectrum of A_0^- was generated assuming an isotropic *g*-value of 2.0035 and linewidth of 13 G.

Time-resolved EPR—The set-up for time-resolved EPR has been described (33). However, in contrast to the out-of-phase ESEEM experiment described therein, weak selective 90° and 180° pulses were used to record the echo-detected spectra. Briefly, spectra were recorded as field-swept echo spectra using the following sequence: laser flash, t_1, 90° microwave pulse, t_2, 180° pulse, t_2, echo. After signal accumulation over several laser shots at a fixed magnetic field, the field was shifted and signal acquisition was repeated in order to construct the EPR spectrum of the transient P_{700}^+ A_1^- state.

Flash Absorption Spectroscopy—Flash-induced absorption changes on a nanosecond time scale were measured as described previously (34), except that a laser diode emitting at 820 nm (SDL-5411-G1 from Spectra Diode Laboratories) was used as measuring light source. Excitation flashes at 532 nm were provided by a neodymium/yttrium-aluminum-garnet laser from Quantel (pulse duration, 300 ps; pulse energy, ~200 μJ/cm^2; repetition rate, 1 Hz). The electronic bandwidth of the detection

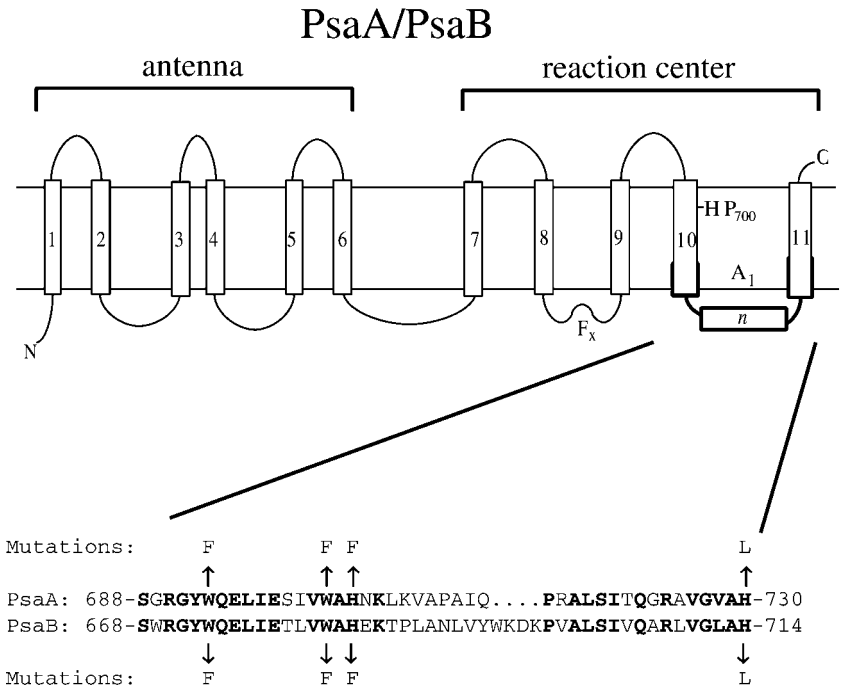

FIG. 1. **Scheme of mutations.** The 11 transmembrane α-helices are indicated as *boxes*; the first 6 serve primarily to bind antenna pigments, while the last 5 surround the reaction center cofactors. The regions responsible for binding the F_X cluster and the histidine serving as the axial ligand to P_{700} are indicated. Note that the 11th α-helix is physically located between helices 9 and 10 (12). The targeted region is *bold*. The *sequences* of the relevant portions of the PsaA and PsaB polypeptides are indicated with the one-letter code as well as the amino acid numbers corresponding to the first and last residue shown (using the *C. reinhardtii* numbering system) in the *lower half* of the figure. The mutations are indicated by an *arrow* from the targeted amino acid to the substituted amino acid.

system (photodiode FND100 from EG&G, AC-coupled amplifier IV72A from the Hahn Meitner Institut (Berlin, Germany), and digital oscilloscope DSA602A with plug-in 11A52 from Tektronix) was 100–500 MHz. For measurements on a millisecond time scale, the photodiode was loaded with a 1-kiloohm resistor and coupled directly to the 11A33 plug-in of the digital oscilloscope. PS1 particles were diluted in 10 mM Tricine (pH 8) and supplemented with 10 mM sodium ascorbate and 10 μM phenazine methosulfate (PMS).

RESULTS

Rationale of Mutagenesis

Site-directed mutagenesis was used to survey the primary structure of the PsaA and PsaB polypeptides for residues that form part of the phylloquinone-binding sites. An extended region from the middle of helix 10 to the middle of helix 11 (Fig. 1) was targeted, as this region would be nearest to the electron densities assigned to phylloquinones in the 4-Å crystal structure (23), and it is analogous to the position in the polypeptides of the bacterial type 2 reaction center where its quinones are bound (35). Only residues that are conserved among all species and between all PsaA and PsaB polypeptides were mutated, given that both polypeptides must provide a niche for a phylloquinone. Based upon the results of ESEEM spectroscopy (20), nitrogen-containing aromatic residues were converted to phenylalanines. In this region there are two tryptophans and two histidines that are conserved between PsaA and PsaB (see Fig. 1). The more drastic change to leucine was made in the case of the second pair of histidines, because these mutations had already been made in a previous study (31). In addition, we constructed double mutants in which homologous residues were both mutated. In the interests of brevity, we have used the following nomenclature for double mutants: "W693F/W673F" refers to the PsaA-W693F/PsaB-W673F double substitution mutant, and the others likewise.

Mutant genes were introduced into strains lacking the corresponding gene (*psaA*, *psaB*, or both) in order to eliminate the possibility of contaminating wild-type sequences. For biophysical analyses, the mutant PS1s were expressed in strains lacking PS2 and Chl *b*, which causes a significant drop in the accumulation of antenna complexes (36). This allowed the EPR analyses to be performed with purified thylakoid membranes, avoiding potential complications caused by detergent extraction of reaction centers.

In Vivo Characterization of Mutants

Growth Characteristics—Growth of the double mutants was tested under several different conditions (Fig. 2). All were capable of heterotrophic growth on acetate media, but under high illumination the W702F/W682F mutant grew poorly. The phenomenon of light sensitivity in PS1 mutants requires the presence of oxygen (37). If grown phototrophically in microaerobic conditions, all the double mutants grew as well as the WT strain, indicating that the mutant PS1s were functional. The mutants W693F/W673F and H704F/H684F could grow under medium light but died under high light, whereas W702F/W682F was killed by even moderate illumination. These defects are likely due to lowered accumulation of PS1 in the mutant strains (Fig. 2), and only in the most demanding conditions, when PS1 function is needed for both photosynthesis and light resistance, does it become limiting. The H730L/H714L mutation caused no observable growth defects (Fig. 2). The single mutants PsaA-W693F and PsaB-W673F were also capable of growth in all conditions (data not shown).

In Vivo Fluorescence Induction Kinetics—The drop in variable fluorescence after the peak during the first seconds of illumination can be used as an indicator for the ability of PS1 (in concert with cytochrome b_6f) to oxidize the plastoquinone pool (38). The extent and speed to which the fluorescence level fell in the double mutants was intermediate between the null mutant and the WT and correlated with their phototrophic growth capability (data not shown). It therefore seems likely that deficiencies in photosynthetic growth are due to the decreased efficiency of electron throughput through cytochrome b_6f and PS1.

Oxygen Evolution—The maximum efficiency of PS2 *in vivo* was assayed directly by suspending cells in bicarbonate buffer and measuring light-driven O_2 evolution using a Clarke-type oxygen electrode. All O_2 evolution was inhibited by addition of 3-(3,4-dichlorophenyl)-1,1-dimethylurea (data not shown). In order to see if O_2 evolution was limited by activities downstream of PS2, *p*-benzoquinone was added to serve as a PS2

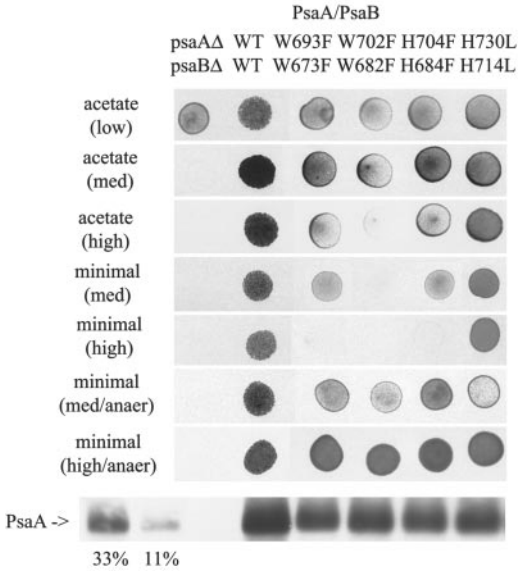

FIG. 2. **Growth characteristics of the double mutant strains.** The indicated strains were grown in liquid culture in acetate-containing medium under low light before spotting onto agar plates. The identity of each strain is indicated at the *top*. Acetate-containing medium allows heterotrophic or mixotrophic growth; minimal medium demands photosynthetic growth. In *parentheses* are indicated the illumination intensities used (see "Experimental Procedures"). The *bottom row* is the result of an immunoblot using anti-PsaA antiserum. Each lane was loaded with the equivalent of 0.5 μg of Chl from solubilized crude membranes. *Lanes* marked *33%* and *11%*represent serial 3-fold dilutions of the WT extract into the *psaA*Δ/*psaB*Δ extract, and allow quantification of PsaA.

acceptor. The mutants were not drastically affected in their ability to photo-oxidize the plastoquinone pool by this test (Table I and data not shown).

Biochemical Characterization of Mutant PS1s

In Vitro Electron Transport Assays—PS1 activity in membranes was measured using ascorbate/2,6-dichlorophenol indophenol as donors and methyl viologen as an acceptor. All of the double mutants had about half the PS1 activity of WT, which correlated with the amount of PsaA detected immunologically (Table I and data not shown).

Multisubunit Immunoblots—To determine whether any of the mutations cause the loss of one or more subunits, quantitative immunoblots were performed with antibodies raised against PsaA, PsaC, PsaD, PsaE, and PsaF. Although all of the double mutants had a lower level of PS1 in their thylakoid membranes (~50% of WT), each of the subunits was present in the same stoichiometry as in WT (data not shown).

Biophysical Measurements

EPR Spectroscopy of Photo-accumulated A_1^-—The A_1^- radical was generated in thylakoid preparations of the double mutants by photo-accumulation. This procedure always produces some contamination from photo-accumulated A_0^- in *Chlamydomonas* membranes. Although the EPR signals of A_0^- and A_1^- cannot be resolved at X-band frequencies (9.4 GHz), they are partially resolved at Q-band frequencies (34 GHz; see Fig. 3, *traces A* and *B*). The phyllosemiquinone anion radical has a *g* anisotropy that is partially resolvable at this frequency (15), whereas much higher microwave frequencies (>250 GHz) are required to resolve the *g*-anisotropy of Chl cations (39) and anions (40). At Q-band frequencies, the low field peak (g_{xx}) of the A_1^- *g*-tensor is well resolved from A_0^- (see Fig. 3, *traces A* and *B*) and gives rise to an asymmetric signal that can be considered diagnostic for an A_1^- + A_0^- mixed spectrum (see

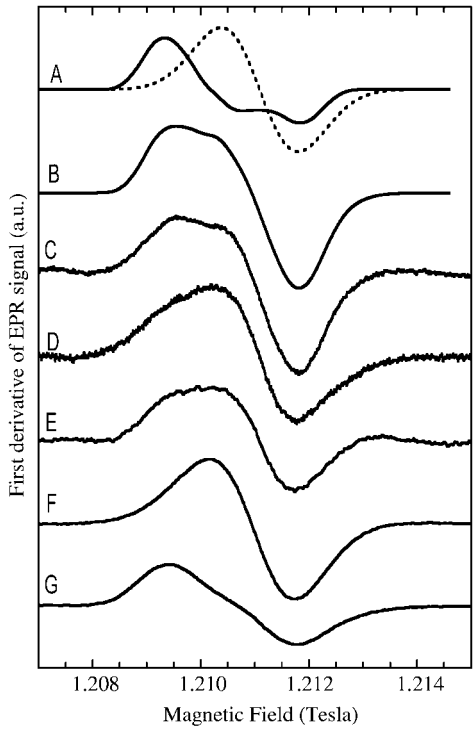

FIG. 3. **Q-band EPR spectra of photo-accumulated A_1^- in thylakoid membranes.** Samples were reduced with sodium dithionite at pH 8 for 30 min in the dark at room temperature, illuminated for 30 min at 200 K, left in the dark at 200 K for 5 min, and stored at 77 K. Spectra were collected at 80 K in the dark (microwave frequency = 34.00 GHz, power = 6 microwatts, modulation frequency = 10 kHz, modulation amplitude = 0.35 milliTesla). Accumulations of three scans are shown. *A*, simulated Q-band spectra of A_1^- (*solid trace*) and A_0^- (*dotted trace*) generated with Bruker SimFonia (see "Experimental Procedures"); *B*, addition of the two simulated spectra in *trace A* (at a ratio of 1:1); *C*, WT; *D*, W702F/W682F; *E*, W693F/W673F; *F*, PsaA-W693F; *G*, PsaB-W673F.

Fig. 3, *traces C* and *D*). Note that the larger *g*-anisotropy of A_1^- causes it to have an apparently weak signal compared with A_0^-. This combined with the somewhat variable photo-accumulation of A_0^- accounts for slight differences in the shapes of our spectra, as has been seen previously (41). Nonetheless, this asymmetric EPR signal serves as a sensitive indicator of A_1^-.

An A_1^- EPR signal was observed in all double mutants except W693F/W673F after a 10-min illumination at pH 10.0 and 200 K (data not shown). As the absence of an A_1^- EPR signal in the W693F/W673F mutant might reflect its double reduction to the EPR-invisible quinol form, the photo-accumulation protocol was modified in order to diminish the probability of double reduction. Photo-accumulations were thus performed under less reducing conditions (pH 8; Ref. 41) for longer time (30 min). Fig. 3 presents Q-band EPR spectra of the various mutants after this protocol. As seen at pH 10, the other tryptophan double mutant (W702F/W682F; Fig. 3*D*) displayed a mixed A_0^- + A_1^- EPR spectrum; the two histidine double mutants looked similar (data not shown). The only difference provoked by the two protocols was that it was possible to photo-accumulate a broad EPR signal resembling a mixture of A_0^- + A_1 in the W693F/W673F mutant at pH 8 (Fig. 3*E*). The single mutants were also examined to see if the phenotype of W693F/W673F was due to both or only one of the mutations. A symmetric spectrum that appeared to arise strictly from A_0^- was observed in the PsaA-W693F mutant; no signals attributable to A_1^- were seen in this mutant at either pH 8 (Fig. 3*F*) or pH 10 (data not shown). In the PsaB-W673F single mutant, the opposite situation was observed; a high A_1^-:A_0^- ratio was reproducibly observed in samples from this mutant at both pH

TABLE I
Normalized in vivo O_2 evolution rates and in vitro O_2 consumption rates

Mutation	*In vivo* O_2 evolution rate[a] (μmol min^{-1} mg Chl^{-1})		O_2 evolution rate[b]	*In vitro* O_2 uptake rate[c]	Amount of PsaA[d]
	− pBQ	+ pBQ			
			% of max	*% WT*	*% WT*
WT	0.89 ± 0.09	1.51 ± 0.08	59 ± 8	100 ± 3	100[d]
*psaA*Δ *psaB*Δ	−0.03 ± 0.01	0.13 ± 0.01	(<0)	0	0[d]
W693F/W673F	0.73 ± 0.11	1.21 ± 0.07	60 ± 9	51 ± 5	46 ± 9
PsaA-W693F	1.34 ± 0.21	1.87 ± 0.11	72 ± 7	93 ± 19	97 ± 20
PsaB-W673F	1.10 ± 0.08	1.18 ± 0.01	93 ± 8	96 ± 19	86 ± 14

[a] The maximum light-dependent O_2 evolution rates of whole cells were measured in 12.5 mM bicarbonate before and after addition of 250 μM *p*-benzoquinone (+ pBQ).
[b] The O_2 evolution rate is expressed as a fraction of the maximum rate (observed in the presence of *p*-benzoquinone).
[c] The maximum light-dependent O_2 uptake rates of crude membrane samples from each mutant were measured with ascorbate/2,6-dichlorophenol indophenol as electron donors and methyl viologen as acceptor. The rates were obtained by a double-reciprocal plot of O_2 uptake rates *versus* light intensity and are expressed relative to that of the WT (100% = 6.22 μmol min^{-1} mg Chl^{-1}).
[d] The amount of PsaA relative to the WT was determined by quantitative immunoblots from the same crude membranes used to measure O_2 uptake rates (normalized to Chl content). The signals from the *psaA*Δ *psaB*Δ and WT strains were defined as 0 and 100%, respectively, for each immunoblot.

8 (Fig. 3*G*) and pH 10 (data not shown). Thus, the point mutation PsaA-W693F has a specific effect on the ability to photoaccumulate the A_1^- radical in a stable manner. The rest of this study focused on the W693F/W673F double mutant and the corresponding single mutants.

Time-resolved X-band EPR—Time-resolved EPR has the advantage of observing the formation of the radical pair P_{700}^+ A_1^- in an unmodified system. Time-resolved X-band pulsed EPR spectroscopy was performed at 80 K on samples of thylakoid membranes. A P_{700}^+ A_1^- spectrum was observed in the WT, single mutants (PsaA-W693F and PsaB-W673F), and the double mutant (Fig. 4). This demonstrates that there is a photo-reducible phylloquinone in PsaA-W693F reaction centers, despite our inability to photo-accumulate A_1^- in them. The P_{700}^+ A_1^- signal persisted for many microseconds after the laser flash in all samples, ruling out an abnormally fast back-reaction from A_1 induced by the mutation(s).

Both the PsaA-W693F mutant and the double mutant exhibited an alteration in a partially resolved hyperfine structure, which is observable as a shoulder on the low field side of the main peak in this spectrum. This feature, which is much more distinct in cyanobacterial PS1, has been attributed primarily to hyperfine couplings from the 2-methyl protons of phylloquinone (19). For reasons not yet fully appreciated, this shoulder is almost invisible in WT *Chlamydomonas* PS1 (Fig. 4; Ref. 19). The P_{700}^+ A_1^- spectrum in the PsaB-W673F mutant appears very similar to WT. The effect of the PsaA-W693F mutation is to make this shoulder better resolved. The specific effect of the PsaA-W693F mutation upon the hyperfine couplings of A_1^- suggests that PsaA-Trp^{693} is close to the phylloquinone normally involved in reversible charge separation at low temperature.

Laser Flash Absorption Spectroscopy—Formation and decay of P_{700}^+ were examined in PS1 particles to assess the stability of charge separation. Photochemistry was initiated by a laser flash, and absorption changes were monitored with a time resolution of up to 2 ns at 820 nm, where P_{700}^+ shows a broad absorption band. A fast, instrument-limited rise in absorbance at 820 nm was observed upon the flash, and it decayed with multiphasic kinetics. In all of the reaction center preparations studied, the most prominent decay occurred on a 5–200-ms time scale, indicating that the long-lived state P_{700}^+ $(F_AF_B)^-$ had been formed (see below). In addition, minor decay phases with $t_{½} \approx$ 2 ns, 30 ns, and 3 μs were detected. Based on previous data (42, 43) and on the observation that the 2-ns and 3-μs phases were preserved upon pre-oxidation of P_{700} (data not shown), we attribute the 2-ns phase to the decay of the excited singlet state and the 3-μs phase to the decay of the triplet state of uncoupled antenna chlorophylls. These two phases were thus ignored for further analysis of the P_{700}^+ kinetics. The 30-ns phase (see Fig. 5, *inset*) most likely reflects charge recombination in the primary pair P_{700}^+ A_0^- (43, 44), indicating that a fraction of the reaction centers (less than ~25% for all mutants studied; Table II) lacked active phylloquinone, so that electron transfer beyond the primary acceptor A_0 was blocked. Note that this fraction does not seem to correlate with the mutations (the WT and double mutant are indistinguishable in this regard; Table II), and it is most likely overestimated by this measurement, due to the contribution of

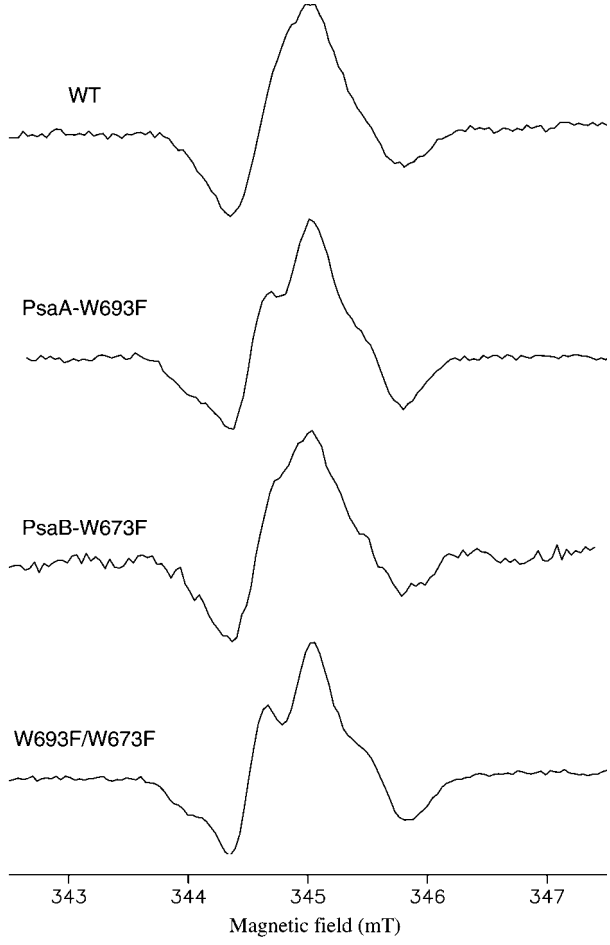

FIG. 4. **Time-resolved EPR spectra of P_{700}^+ A_1^- in PS1 from the WT and the Trp mutants (PsaA-W693F, PsaB-W673F, PsaA-W693F/PsaB-W673F).** See text for details.

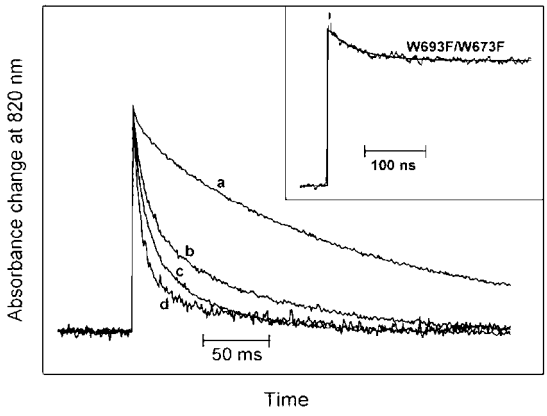

FIG. 5. **P_{700}^+ re-reduction observed by flash absorption spectroscopy at 820 nm.** Comparison of WT (*trace a*) and the mutants PsaA-W693F (*trace b*), PsaB-W673F (*trace c*), and W693F/W673F (*trace d*) in the millisecond time scale. Signal amplitudes were normalized for ease of comparison. *Inset*, kinetics in the nanosecond time scale. *Noisy line*, experimental data; *smooth line*, least squares fit to a mono-exponential decay ($t_{½}$ = 34 ns) plus a constant. The data during the first 7 ns after excitation (positive spike attributed to singlet excited Chls; see text) were not taken into account for the fit.

TABLE II
The kinetics of in vitro P_{700}^+ re-reduction of PS1 particles
Samples were excited by laser flashes at 532 nm, and the absorption changes were monitored at 820 nm.

Strain	Fraction of ΔA_{820} decaying with $t_{½} \approx 30$ ns[a]	Initial rate of slow component[b]
	%	s^{-1}
WT	18	10
PsaA-W693F	26	50
PsaB-W673F	12	72
W693F/W673F	20	122

[a] Absorption changes decaying within less than 5 ns (attributed to singlet excited Chls) and with $t_{½} \approx 3$ μs (attributed to triplet states) were not taken into account for the calculation of this fraction.
[b] The initial rates were determined by bi-exponential fits to the signals shown in Fig. 5.

A_0^- to the transient absorption at 820 nm.

Surprisingly, we found that mutation of either PsaA-Trp^{693} or PsaB-Trp^{673} caused a strong acceleration of the rate of P_{700}^+ re-reduction occurring in the millisecond time scale (Fig. 5). Under these experimental conditions, P_{700}^+ re-reduction occurring in this time regime is due to a combination of electron donation from reduced PMS in the medium and a back-reaction (charge recombination) from $(F_A/F_B)^-$, the terminal iron-sulfur clusters. The kinetics deviate from a mono-exponential decay of P_{700}^+, because partial electron escape from $(F_A/F_B)^-$ to acceptors present in the medium produces a fraction of reaction centers where electron donation from PMS no longer competes with charge recombination (45). The initial rate of P_{700}^+ decay, however, should represent the sum of the rate constants of charge recombination and of electron donation by PMS. The initial rates calculated from curve fitting of the observed P_{700}^+ kinetics show an acceleration (compared with WT) by a factor of about 5, 7, and 12 in the mutants PsaA-W693F, PsaB-W673F, and W693F/W673F, respectively (Table II). Because these mutations should be far from P_{700}, we do not expect them to have a large effect upon electron donation from reduced PMS to P_{700}^+. Thus, the observed acceleration of the initial rate by the mutations should be primarily through increasing the rate of charge recombination between P_{700}^+ and $(F_A/F_B)^-$.

DISCUSSION

We conclude that the indole of PsaA-Trp^{693} is part of the A_1 phylloquinone-binding site. Although indirect effects of its mutation could be invoked to explain the effects of its mutation, this seems unlikely given that six other mutations in the same general region did not produce similar effects. Moreover, the effect of the PsaA-W693F mutation is most easily explained by changes in the immediate environment of the phylloquinone (see below). This conclusion is in agreement with the prediction based on molecular modeling by Kamlowski *et al.* (46), but is in disagreement with a recent prediction based upon conserved sequence motifs (47), in which the downstream tryptophans were implicated. Our results are also in general agreement with recently published data (48), in which mutation of PsaA-Trp^{693} to His or Leu altered the ENDOR spectrum of A_1^- and slowed decay of the spin-polarized P_{700}^+ A_1^- signal. However, these mutants seemed to be able to photo-accumulate an A_1^- radical, as seen by X-band EPR (48); we do not understand the apparent discrepancy with our results using the less drastic PsaA-W693F mutant.

The effects of mutation of this tryptophan can now be rationalized in light of the new higher resolution crystal structure of cyanobacterial PS1 (12). The tryptophan shown here to affect the A_1^- EPR signal is now clearly seen to π-π stack with the phylloquinone bound to PsaA, whereas the symmetry-related phylloquinone is similarly stacked with the analogous tryptophan in PsaB (12). In this arrangement, the planes of the naphthoquinone and indole moieties are almost parallel, with the five-membered ring of the indole over the quinone ring and the six-membered ring of indole over the 2-methyl group of the quinone (12). It is gratifying that our results, obtained from a systematic genetic approach, so accurately pinpointed the aromatic residue forming a key part of the A_1 binding site. It seems very likely that the nitrogen of PsaA-Trp^{693} is the one observed by ESEEM spectroscopy of photo-accumulated A_1^- (20), as this residue both π-stacks with the quinone and partially overlaps it (12), as predicted from those experiments (20). Unfortunately, our inability to photo-accumulate an A_1^- radical in the PsaA-W693F mutant precludes us from testing this directly. Although it is true that the crystal structure alone cannot determine which quinone is used in electron transfer, the structural constraints provided by the structure make a prediction. We know that the chlorophyll ligated by PsaB-His^{656} carries most of the spin in the photo-accumulated P_{700}^+ cation radical from EPR and ENDOR measurements of site-directed mutants (25, 49, 50) and that the distance between P_{700}^+ and A_1^-, as measured by pulsed EPR of the radical pair in crystals at 80 K, is 25.4 ± 0.3 Å (22). Based on the crystal structure, the center-to-center distances from the B-side P_{700} chlorophyll to the A-side and B-side phylloquinones is 26.0 ± 0.3 and 24.4 ± 0.3 Å (12), respectively, making it more likely that the A-side quinone is the one seen by time-resolved EPR at low temperature. However, considering the uncertainties of these measurements and the fact that the EPR out-of-phase echo experiment is not necessarily measuring center-to-center distances, this conclusion is far from iron-clad. By examining the time-resolved EPR spectra of tryptophan mutants on both sides and finding that only the PsaA-W693F mutation had an effect, the prediction posed by the structural and EPR data has now been tested and confirmed.

The PsaA-W693F mutation caused a loss of the stable A_1^- EPR signal. We considered two explanations: loss of phylloquinone from the altered site prior to EPR analysis or double reduction to the EPR-silent phylloquinol during the photo-accumulation protocol. We do not favor the former for several reasons. First, forward electron transfer from A_1 to F_X in this mutant has been observed *in vivo* by laser-flash spectroscopy (51). Second, a flash-induced P_{700}^+ A_1^- EPR signal demonstrated the presence of phylloquinone active in charge separa-

tion in thylakoid membranes. Third, the upper limit of the population producing a back reaction from A_0 in detergent-solubilized PS1 particles was estimated to be ~25% by time-resolved absorption spectroscopy. Finally, the phylloquinone content of these particles was measured directly by solvent extraction of pigments and liquid chromatography/mass spectrometry, and the amount of phylloquinone per P_{700} in the PsaA-W693F sample was estimated to be ~80% that of the WT (data not shown; see "Experimental Procedures"). Conversion of the phylloquinone in the altered site to phylloquinol during photo-accumulation presumably is due to easier access of protons to the semiquinone. PsaA-Trp^{693} forms part of the phylloquinone-binding pocket that shields the quinone (and semiquinone) from aqueous solvent, which may partially explain why the midpoint potential of A_1 is so much lower than phylloquinone *in vitro*. The availability of protons would allow the otherwise unfavorable (52) double reduction of phylloquinone to the stable phylloquinol. This might also explain why no A_1^- EPR signal was seen when the pH was lowered from 10 to 8; although this decreases the reducing power of the dithionite, it increases the proton concentration by 100-fold. Loss of the photo-accumulated A_1^- EPR signal was also observed in cyanobacterial mutants lacking PsaF (16), and similar reasoning was used to suggest that the active phylloquinone was closest to PsaF (see Ref. 16 for a detailed discussion). The phenotype of A_1 double-reduction upon either loss of PsaF or mutation of PsaA-Trp^{693} is consistent with the placement of the PsaA-Trp^{693} on the side of PS1 closest to PsaF (12).

The change to the environment of the phylloquinone upon conversion of the nearby indole group to a phenyl ring might explain several of the effects seen in the PsaA-W693F mutant. We observed a significant modification of the time-resolved $P_{700}^+ A_1^-$ EPR spectrum in this mutant and in the W693F/W673F double mutant. Somewhat paradoxically, this altered spectrum resembles more closely the spectrum from WT PS1 in cyanobacteria, where the low field shoulder attributed mainly to hyperfine couplings with the 2-methyl protons is more prominent (19). At this time, the cause of this effect is unclear. It might be that the hyperfine couplings of the methyl protons themselves or other couplings have shifted, allowing a better resolution of this feature. An interesting possibility is that the removal of the indole nitrogen by mutation removes a ^{14}N coupling to the phylloquinone radical. The latter interpretation seems more compatible with fact that the time-resolved proton ENDOR spectrum of the radical pair in the PsaA-W693F mutant closely resembles that of the wild type.[2] Increased hydrophilic character around the A_1 phylloquinone after loss of the larger indole would also be expected to increase its redox midpoint potential (*i.e.* stabilize the semiquinone), which would decrease the driving force of electron transfer from A_1 to F_X. One prediction of this hypothesis would be a decrease in the rate of forward electron transfer from A_1 to F_X, which has been observed (51). The second prediction would be an acceleration of charge recombination in the pair $P_{700}^+ (F_A/F_B)^-$, because this recombination presumably involves an uphill reverse electron transfer from $(F_A/F_B)^-$ to A_1 (53). The acceleration that was observed (see Table II) would be consistent with an increase of the effective reduction potential of A_1 by ~60 mV for the two single mutants and ~80 mV for the double mutant.

This last point immediately raises the question: is a unique phylloquinone active or are both active in charge separation? Mutation of either PsaA-Trp^{693} or PsaB-Trp^{673} increased the initial rate of P_{700}^+ re-reduction severalfold, and the W693F/W673F double mutant exhibited a back-reaction that was significantly faster than the PsaA-W693F single mutant alone. This would indicate that charge recombination can make use of the branch of cofactors that include the phylloquinone near PsaB-Trp^{673}. The mutation may either accelerate an existing reaction or open a new pathway. Other recent data are consistent with the hypothesis that both phylloquinones are active in forward electron transfer. Joliot and Joliot (11) observed two kinetic components associated with electron transfer from the phylloquinone(s) by *in vivo* laser flash spectroscopy. It was recently found that the PsaB-W673F mutation specifically affected the faster kinetic component ($t_{1/2}$ = 13 ns), whereas the PsaA-W693F mutation specifically affected the slower kinetic component ($t_{1/2}$ = 140 ns; Ref. 51). Additionally, the FTIR spectrum of $P_{700}^+ A_1^-$ in the absence of Fe-S clusters is consistent with reduction of two quinones in different environments (54). The new structural information has allowed predictions about several potential sources of difference between the two phylloquinone sites, including residues not conserved between PsaA and PsaB, and nearby lipids (anionic phosphatidylglycerol near the A-side quinone and neutral galactolipid near the B-side quinone; Ref. 12).

Despite the above, the simplest interpretation of the EPR data shown here is that charge separation is unidirectional and leads to reduction of the phylloquinone closest to PsaA-Trp^{693} ("$A_{1(A)}$"). However, it may not normally be possible to accumulate a semiquinone in the other site ("$A_{1(B)}$"); in the presence of the three reduced Fe-S clusters, $A_{1(B)}$ may become more difficult to reduce than $A_{0(B)}$. The PsaB-W673F mutation may stabilize $A_{1(B)}^-$, consistent with its acceleration of charge recombination (Table II) and its retardation of electron transfer to F_X (51), allowing stable accumulation of an $A_{1(B)}^-$ radical rather than $A_{0(B)}^-$. This hypothesis allows us to explain two observations that are difficult to reconcile with a model in which $A_{1(A)}$ represents the only photo-active quinone. The first is that it is possible to photo-accumulate an A_1^- signal in the W693F/W673F double mutant under conditions where only A_0^- is observed in the PsaA-W693F single mutant; the prediction is that this additional signal represents $A_{1(B)}^-$. The second is the observation of a reproducibly stronger photo-accumulated A_1^- signal with very little contaminating A_0^- in the PsaB-W673F single mutant; the prediction is that this spectrum actually represents the superposition of $A_{1(A)}^-$ and $A_{1(B)}^-$. Analysis of these radicals under high field conditions, where the *g*-tensors of semiquinones in different environments should be resolved, will be required to test this hypothesis. The lack of effect of the PsaB-W673F mutation upon the time-resolved $P_{700}^+ A_1^-$ EPR signal at 80 K is most easily explained by the assumption that $A_{1(B)}$ is not involved in charge separation under these conditions. An alternative, albeit unlikely, explanation is that the time-resolved spectrum in *Chlamydomonas* represents the superposition of $P_{700}^+ A_{1(A)}^-$ and $P_{700}^+ A_{1(B)}^-$, but the PsaB-W673F mutation does not have an observable effect on the hyperfine couplings to $A_{1(B)}^-$. However, low temperature measurements of cyanobacterial PS1 crystals are not consistent with a significant superposition of two differently oriented $P_{700}^+ A_1^-$ pairs (22).

Acknowledgments—We thank John Vincent and Stephen Woski for critical reading of the manuscript, W. Lubitz (Technische Universität Berlin, Berlin, Germany) for the possibility to record the time-resolved EPR spectra, and Bruker Analytik GmbH for use of their Q-band EPR spectrometer. K. R. acknowledges support from Bill Rutherford for ideas and encouragement during the early stages of this project.

REFERENCES

1. Fish, L. E., Kück, U., and Bogorad, L. (1985) *Molecular Biology of the Photosynthetic Apparatus*, pp. 111–120, Cold Spring Harbor Laboratory, Cold Spring Harbor, NY
2. Vallon, O., and Bogorad, L. (1993) *Eur. J. Biochem.* **214,** 907–915
3. Brettel, K. (1988) *FEBS Lett.* **239,** 93–98

[2] R. Bittl and K. Redding, unpublished results.

4. Bock, C. H., Van der Est, A. J., Brettel, K., and Stehlik, D. (1989) *FEBS Lett.* **247,** 91–96
5. Moenne-Loccoz, P., Heathcote, P., Maclachlan, D. J., Berry, M. C., Davis, I. H., and Evans, M. C. (1994) *Biochemistry* **33,** 10037–10042
6. van der Est, A., Bock, C., Golbeck, J., Brettel, K., Setif, P., and Stehlik, D. (1994) *Biochemistry* **33,** 11789–11797
7. Leibl, W., Toupance, B., and Breton, J. (1995) *Biochemistry* **34,** 10237–10244
8. Mathis, P., and Setif, P. (1988) *FEBS Lett.* **237,** 65–68
9. Setif, P., and Brettel, K. (1993) *Biochemistry* **32,** 7846–7854
10. Brettel, K. (1998) in *Photosynthesis: Mechanism and Effects, Proceedings of the 11th International Congress of Photosynthesis* (Garab, G., ed.) Vol. 1, pp. 611–614, Kluwer Academic Publishers, Dordrecht, Netherlands
11. Joliot, P., and Joliot, A. (1999) *Biochemistry* **38,** 11130–11136
12. Jordan, P., Fromme, P., Witt, H. T., Klukas, O., Saenger, W., and Krauss, N. (2001) *Nature* **411,** 909–917
13. Rustandi, R. R., Snyder, S. W., Feezel, L. L., Michalski, T. J., Norris, J. R., Thurnauer, M. C., and Biggins, J. (1990) *Biochemistry* **29,** 8030–8032
14. Heathcote, P., Hanley, J. A., and Evans, M. C. W. (1993) *Biochim. Biophys. Acta* **1144,** 54–61
15. MacMillan, F., Hanley, J., van der Weerd, L., Knuepling, M., Un, S., and Rutherford, A. W. (1997) *Biochemistry* **36,** 9297–9303
16. Yang, F., Shen, G., Schluchter, W. M., Zybailov, B. L., Ganago, A. O., Vassiliev, I. R., Bryant, D. A., and Golbeck, J. H. (1998) *J. Phys. Chem. B* **102,** 8288–8299
17. Rigby, S. E. J., Evans, M. C. W., and Heathcote, P. (1996) *Biochemistry* **35,** 6651–6656
18. Teutloff, C., MacMillan, F., Bittl, R., Lendzian, F., and Lubitz, W. (1998) in *Photosynthesis: Mechanism and Effects, Proceedings of the 11th International Congress of Photosynthesis* (Garab, G., ed.) Vol. 1, pp. 607–610, Kluwer Academic Publishers, Dordrecht, Netherlands
19. Bittl, R., Zech, S. G., Teutloff, C., Krabben, L., and Lubitz, W. (1998) in *Photosynthesis: Mechanism and Effects, Proceedings of the 11th International Congress of Photosynthesis* (Garab, G., ed) Vol. 1, pp. 509–514, Kluwer Academic Publishers, Dordrecht, Netherlands
20. Hanley, J., Deligiannakis, Y., MacMillan, F., Bottin, H., and Rutherford, A. W. (1997) *Biochemistry* **36,** 11543–11549
21. Zech, S. G., van der Est, A. J., and Bittl, R. (1997) *Biochemistry* **36,** 9774–9779
22. Bittl, R., Zech, S. G., Fromme, P., Witt, H. T., and Lubitz, W. (1997) *Biochemistry* **36,** 12001–12004
23. Klukas, O., Schubert, W. D., Jordan, P., Krau, N., Fromme, P., Witt, H. T., and Saenger, W. (1999) *J. Biol. Chem.* **274,** 7361–7367
24. Picard, V., Ersdal-Badju, E., Lu, A., and Bock, S. C. (1994) *Nucleic Acids Res.* **22,** 2587–2591
25. Redding, K., MacMillan, F., Leibl, W., Brettel, K., Rutherford, A. W., Breton, J., and Rochaix, J. D. (1998) in *Photosynthesis: Mechanism and Effects, Proceedings of the 11th International Congress of Photosynthesis* (Garab, G., ed.) Vol. 1, pp. 591–594, Kluwer Academic Publishers, Dordrecht, Netherlands
26. Harris, E. H. (1989) *The Chlamydomonas Sourcebook: A Comprehensive Guide to Biology and Laboratory Use*, Academic Press, Inc., San Diego
27. Ohad, I., Adir, N., Koike, H., Kyle, D. J., and Inoue, Y. (1990) *J. Biol. Chem.* **265,** 1972–1979
28. Fischer, N., Setif, P., and Rochaix, J. D. (1997) *Biochemistry* **36,** 93–102
29. Porra, R., Thompson, W., and Kriedemann, P. (1989) *Biochim. Biophys. Acta* **975,** 384–394
30. Takahashi, Y., Goldschmidt-Clermont, M., Soen, S. Y., Franzen, L. G., and Rochaix, J. D. (1991) *EMBO J.* **10,** 2033–2040
31. Redding, K., MacMillan, F., Leibl, W., Brettel, K., Hanley, J., Rutherford, A. W., Breton, J., and Rochaix, J. D. (1998) *EMBO J.* **17,** 50–60
32. Patzlaff, J. S., and Barry, B. A. (1996) *Biochemistry* **35,** 7802–7811
33. Bittl, R., and Zech, S. G. (1997) *J. Phys. Chem. B* **101,** 1429–1436
34. Kusumoto, N., Setif, P., Brettel, K., Seo, D., and Sakurai, H. (1999) *Biochemistry* **38,** 12124–12137
35. Deisenhofer, J., and Michel, H. (1989) *EMBO J.* **8,** 2149–2170
36. Allen, K. D., and Staehelin, L. A. (1994) *Planta* **194,** 42–54
37. Rochaix, J., Fischer, N., and Hippler, M. (2000) *Biochimie* (*Paris*) **82,** 635–645
38. Bennoun, P., and Delepelaire, P. (1982) in *Methods in Chloroplast Molecular Biology* (Edelman, M., Hallick, R. B., and Chua, N.-H., eds) pp. 25–38, Elsevier Biomedical Press, Amsterdam
39. MacMillan, F., Rohrer, M., Krzystek, J., Brunel, L. C., and Rutherford, A. W. (1998) in *Photosynthesis: Mechanism and Effects, Proceedings of the 11th International Congress of Photosynthesis* (Garab, G., ed.) Vol. 2, pp. 715–718, Kluwer Academic Publishers, Dordrecht, Netherlands
40. Dorlet, P., Rutherford, A. W., and Un, S. (2000) *Biochemistry* **39,** 7826–7834
41. Heathcote, P., and Evans, M. C. W. (1980) *FEBS Lett.* **111,** 381–385
42. Brettel, K., and Golbeck, J. H. (1995) *Photosynth. Res.* **45,** 183–193
43. Brettel, K., and Setif, P. (1987) *Biochim. Biophys. Acta* **893,** 109–114
44. Setif, P., Bottin, H., and Mathis, P. (1985) *Biochim. Biophys. Acta* **808,** 112–122
45. Diaz-Quintana, A., Leibl, W., Bottin, H., and Setif, P. (1998) *Biochemistry* **37,** 3429–3439
46. Kamlowski, A., Altenberg-Greulich, B., Van der Est, A., Zech, S. G., Bittl, R., Fromme, P., Lubitz, W., and Stehlik, D. (1998) *J. Phys. Chem. B* **102,** 8278–8287
47. Fisher, N., and Rich, P. R. (2000) *J. Mol. Biol.* **296,** 1153–1162
48. Purton, S., Stevens, D. R., Muhiuddin, I. P., Evans, M. C., Carter, S., Rigby, S. E., and Heathcote, P. (2001) *Biochemistry* **40,** 2167–2175
49. Webber, A. N., Su, H., Bingham, S. E., Kass, H., Krabben, L., Kuhn, M., Jordan, R., Schlodder, E., and Lubitz, W. (1996) *Biochemistry* **35,** 12857–12863
50. Krabben, L., Schlodder, E., Jordan, R., Carbonera, D., Giacometti, G., Lee, H., Webber, A. N., and Lubitz, W. (2000) *Biochemistry* **39,** 13012–13025
51. Guergova-Kuras, M., Boudreaux, B., Joliot, A., Joliot, P., and Redding, K. (2001) *Proc. Natl. Acad. Sci. U. S. A.* **98,** 4437–4442
52. Prince, R. C., Dutton, P. L., and Bruce, J. M. (1983) *FEBS Lett.* **160,** 273–276
53. Jordan, R., Nessau, U., and Schlodder, E. (1998) in *Photosynthesis: Mechanism and Effects, Proceedings of the 11th International Congress of Photosynthesis* (Garab, G., ed.) Vol. 1, pp. 663–666, Kluwer Academic Publishers, Dordrecht, Netherlands
54. Hastings, G., and Sivakumar, V. (2001) *Biochemistry* **40,** 3681–3689